Langmuir

Article

pubs.acs.org/Langmuir

How Does the Surface Charge of Ionic Surfactant and Cholesterol Forming Vesicles Control Rotational and Translational Motion of Rhodamine 6G Perchlorate (R6G ClO_4)?

Surajit Ghosh,[†] Arpita Roy,[†] Debasis Banik,[†] Niloy Kundu,[†] Jagannath Kuchlyan,[†] Anjali Dhir,[‡] and Nilmoni Sarkar*[,†]

[†]Department of Chemistry, Indian Institute of Technology, Kharagpur 721302, West Bengal, India

[‡]Department of Chemistry, Indian Institute of Technology, Bombay, Mumbai 400076, India

Supporting Information

ABSTRACT: The rotational dynamics and translational diffusion of a hydrophilic organic molecule, rhodamine 6G perchlorate (R6G ClO_4) in small unilamellar vesicles formed by two different ionic surfactants, cetyltrimethylammonium bromide (CTAB) and sodium dodecyl sulfate (SDS), with cholesterol have been investigated using fluorescence spectroscopic methods. Moreover, in this article the formation of vesicle using anionic surfactant, SDS at different cholesterol-to-surfactant molar ratio (expressed by Q value (Q = [cholesterol]/[surfactant])) has also been reported. Visual observation, dynamic light scattering (DLS) study, turbidity measurement, steady state fluorescence anisotropy (r_0) measurement, and eventually microscopic images reveal the formation of small unilamellar vesicles in aqueous solution. Also, in this study, an attempt has been made to observe whether the cationic probe molecule, rhodamine 6G (R6G) experiences similar or different microenvironment in cholesterol-SDS and cholesterol-CTAB assemblies with increase in cholesterol concentration. The influence of cholesterol on rotational and translational diffusion of R6G molecules has been investigated by monitoring UV−vis absorption, fluorescence, time-resolved fluorescence anisotropy, and finally fluorescence correlation spectroscopy (FCS) measurements. In cholesterol−SDS assemblies, due to the strong electrostatic attractive interaction between the negatively charged surface of vesicle and cationic R6G molecules, the rotational and diffusion motion of R6G becomes slower. However, in cholesterol−CTAB aggregates, the enhanced hydrophobicity and electrostatic repulsion induces the migration of R6G from vesicle bilayer to aqueous phase. The experimental observations suggest that the surface charge of vesicles has a stronger influence than the hydrophobicity of the vesicle bilayer on the rotational and diffusion motion of R6G molecules.

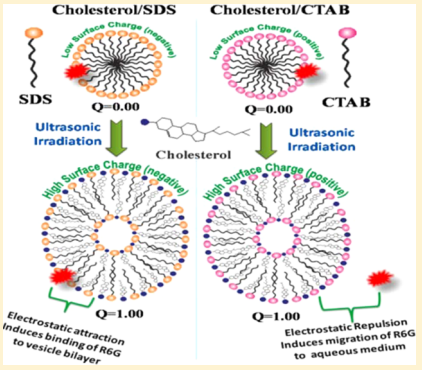

1. INTRODUCTION

Phospholipid-containing vesicles (liposomes) have been studied extensively as a vehicle for drug molecules due to their potential use in entrapment of both hydrophilic and hydrophobic drug molecules.[1−4] In aqueous solution, the formation of multilamellar (aqueous core confined by more than one lipid bilayer) or unilamellar (aqueous core confined by one lipid bilayer) vesicles depends upon the concentration of lipid molecules, preparation methods, etc.[5] However, the degradation of phospholipids by hydrolysis is a major problem in aqueous medium, which decreases the stability of vesicles (liposomes).[6] Additionally, formation of unilamellar vesicles with narrow size distribution is comparatively difficult than multilamellar ones using phospholipids.[5] The methods of preparation of unilamellar lipid vesicles involve several exhaustive steps; therefore, preparation and characterization of small unilamellar vesicles using surfactant molecules as an alternative for phospholipids are interesting research areas in the fields of surface and colloid chemistry. Generally, a single-chain surfactant molecule forms a vesicle in aqueous medium by mixing with oppositely charged surfactant or other organic additives.[7−16] In aqueous solution, self-assemblies of amphiphilic surfactant molecules can form various nanostructures (i.e., spherical micelle, vesicles, or elongated/wormlike micelle) depending upon concentration, the presence of external additives, pH of medium, temperature, etc.[11,14,16−19] These nanostructures of surfactant molecules are able to exhibit colloidal stability and also show potential uses in the field of nanomaterial synthesis, pharmaceutical applications, catalysis, etc.[20−22]

Micelles and vesicles are two important classes of supramolecular assemblies of surfactant molecules in aqueous medium. The transition from surfactant micelles to vesicles in aqueous solution is a unique phenomenon that mimics various biological processes.[23,24] The transition between micelle and vesicle is generally influenced by different external stimuli, such

Received: December 11, 2014
Revised: February 2, 2015
Published: February 2, 2015

DOI: 10.1021/la504819v
Langmuir 2015, 31, 2310−2320

Scheme 1. Structures of Sodium Dodecyl Sulfate (SDS), Cetyl Trimethylammonium Bromide (CTAB), Cholesterol, and Rhodamine 6G ClO_4 (R6GClO_4)

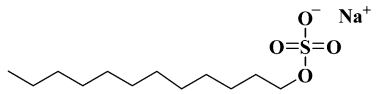

Sodium dodecyl sulfate (SDS)

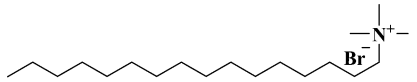

Cetyltrimethylammonium bromide (CTAB)

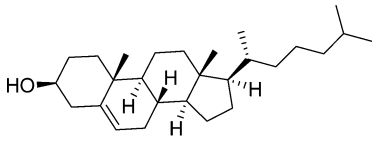

Cholesterol

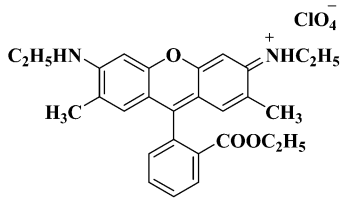

Rhodamine 6G perchlorate (R6G ClO_4)

as polar additives, organic compounds, water-insoluble sterol moieties, etc.[13−15,25−27] In recent times, vesicles formed by a hydrated mixture of surfactant and cholesterol molecules have received much more attention compared to lipid vesicles due to their better stability, easy preparation methods, etc.[13,27−29] Cholesterol molecules are insoluble in water, and therefore synergic interaction with the hydrophobic alkyl chain of surfactant molecules leads to the formation of bilayer structures in aqueous medium.[27] The nonionic surfactant and cholesterol molecule comprising vesicles, termed as "niosomes", have been characterized using various nonionic surfactant molecules.[28,29] Additionally, the hydrated mixture of cationic long alkyl chain-containing amphiphilic molecules is capable of forming unilamellar vesicles in aqueous solution.[13,27,30] Ventosa and coworkers reported the detailed mechanisms regarding the formation of vesicles in aqueous solution of cationic surfactant, cetyltrimethylammonium bromide (CTAB) with increasing cholesterol content.[27] Very recently, we have characterized cholesterol-induced vesicle formation in aqueous solution of 1-hexadecyl-3-methylimidazolium chloride ([C_{16}mim]Cl) and benzyldimethylhexadecylammonium chloride (BHDC).[30] However, to the best of our knowledge, there is no such report related to micelle−vesicle transition in common anionic surfactant solution with the addition of cholesterol.

In this Article, we have characterized micelle−vesicle transition in aqueous solution of the anionic surfactant sodium dodecyl sulfate (SDS) with increase in cholesterol content. In water, SDS molecules form micelles above a certain concentration of surfactant (termed the critical micelle concentration, or cmc). However, in aqueous mixture of these two species at different cholesterol-to-SDS molar ratios (Q = [cholesterol]/[SDS]), a uniform distribution of unilamellar vesicles with an average diameter around the ∼100 nm range is observed. The characterization of cholesterol−SDS mixtures with increasing cholesterol concentration were executed systematically by observing visual changes, turbidity, dynamic light scattering (DLS) study, and transmission electron microscopy (TEM) measurements. The size distribution of DLS profiles and TEM images clearly suggest the formation of highly stable and uniformly shaped unilamellar spherical vesicles.

Cholesterol is insoluble in water, and is therefore located in the bilayer region of vesicles. It is interesting to observe the structural and dynamical properties of these supramolecular assemblies and also their influence on the photophysics of encapsulated probe molecules during the micelle−vesicle transition with increasing cholesterol concentration. Previously, the hydration behavior of water molecules in bilayers of cholesterol−C_{16}mimCl and cholesterol−BHDC forming vesicles had been explored by using coumarin 153 (C-153) as the solvatochromic probe molecule.[30] The solvation time of C-153 increases in vesicles significantly compared to that in micelles due to the decrease in hydration behavior in the vesicle bilayer.[30] Additionally, the photophysical properties of proton transfer molecules 2,2′-bipyridine-3,3′-diol, $BP(OH)_2$ and curcumin have also been compared in two different micro-environments: surfactant micelles and cholesterol−surfactant-containing vesicles.[29,31] It was observed that the confined and rigid environment provided by these vesicles enhanced the fluorescence lifetime as well as the related photophysical properties of proton transfer molecules in vesicles relative to that in micelles.[29,31] These studies revealed that cholesterol molecules increase the hydrophobicity of vesicle bilayers substantially. Moreover, using fluorescence correlation spectroscopic (FCS) techniques, Bhattacharyya and co-workers[32] monitored the diffusion of different organic dye molecules in niosomes composed of nonionic surfactant (Triton X-100) and cholesterol. The salt (sodium chloride, NaCl) effect on the proton transfer dynamics of pyranine in niosomes has also been investigated.[33] In this Article, we are interested in the investigation of the rotational and translational diffusion motion of an amphiphilic organic dye molecule (rhodamine 6G Perchlorate, R6G ClO_4) in ionic surfactant and cholesterol assemblies containing different surface charges.

To investigate the location, rotational dynamics, and translational diffusion of R6G in cholesterol−SDS vesicles with increasing cholesterol concentration, steady-state absorption-emission spectroscopy, time-resolved fluorescence anisotropy, and finally FCS techniques were used. To make a comparison regarding the rotational and diffusion motions of R6G between cationic surfactant−cholesterol- and anionic surfactant−cholesterol-containing vesicles, the same set of experiments were performed in cationic surfactant CTAB−cholesterol-containing aggregates at different Q values. Since R6G is a cationic dye molecule, the interaction with anionic SDS and that with cationic CTAB molecules are expected to be

DOI: 10.1021/la504819v
Langmuir 2015, 31, 2310−2320

different. In this attempt, the fluorescence anisotropy and translational diffusion of R6G were monitored in cholesterol−SDS and cholesterol−CTAB vesicles at various Q values, which enabled us to realize the influence of surface charge of vesicles on the mobility of R6G molecules. Therefore, it will be interesting to find out how the cholesterol concentration and electrostatic interactions are going to influence the solute location in surfactant−cholesterol vesicles.

2. EXPERIMENTAL SECTION

2.1. Materials. SDS and cholesterol were obtained from Sisco Research Laboratories Pvt. Ltd. (SRL), India. CTAB was obtained from Sigma-Aldrich. R6G ClO_4 was purchased from Exciton. Triply distilled Milli-Q water was used to prepare the aqueous solution of surfactant micelle and cholesterol−surfactant vesicles. The concentration of surfactants (SDS and CTAB) was 20 mM.

The structures of SDS, CTAB, cholesterol, and R6G ClO_4 are shown in Scheme 1.

2.2. Instrumentations. *2.2.1. Structural Characterization of Cholesterol and Surfactant-Containing Nanoaggregates.* The size distributions of aqueous SDS solution and cholesterol−SDS nanoaggregates were determined using a Malvern Nano ZS instrument employing a 4 mW He−Ne laser (λ = 632 nm) with detector angle positioned at 173°.

2.2.2. Cryogenic Transmission Electron Microscope (Cryo-TEM) Measurements. The cryo-TEM experiments were performed using a JEM-2100 HRTEM electron microscope equipped with a Gatan cold stage.

2.2.3. Transmission Electron Microscopy Measurements. JEOL model JEM 2010 transmission electron microscope is used for TEM measurements.

2.2.4. Zeta Potential Measurement. The Malvern Nano ZS instrument with 4 mW He−Ne laser (λ = 632 nm) was also used for zeta potential measurement.

2.2.5. Steady State Fluorescence Anisotropy (r_0) Measurement. The changes in steady state anisotropy (r_0) of 1,6-diphenyl-1,3,5-hexatriene (DPH) in cholesterol−surfactant aggregates at different Q values were measured using a PerkinElmer LS-55 spectrofluorimeter. To calculate the steady state anisotropy (r_0), the following equations were used:[34]

$$r_0 = \frac{(I_{VV} - GI_{VH})}{(I_{VV} + 2GI_{VH})} \quad (1)$$

$$G = \frac{I_{HV}}{I_{HH}} \quad (2)$$

where I_{VV} and I_{VH} designate emission intensity polarized parallel and perpendicular to the vertical polarization of the excitation light, respectively. G is the correction factor.

2.2.6. UV−Vis Absorption and Emission Measurements. The UV−visible absorption spectra of R6G ClO_4 molecule were recorded using a Shimadzu spectrophotometer (model number UV-2450). The emission and excitation spectra of R6G ClO_4 were monitored using a Hitachi (model number F−7000) spectrofluorimeter. For steady-state fluorescence experiments, the samples were excited at 440 nm.

2.2.7. Time Resolved Fluorescence Anisotropy Measurements. Time resolved anisotropy measurements were performed using a time correlated single photon counting (TCSPC) picosecond spectrophotometer. Time resolved fluorescence anisotropy is defined by the following equation:[34]

$$r(t) = \frac{I_{\parallel}(t) - I_{\perp}(t)}{I_{\parallel}(t) + 2GI_{\perp}(t)} \quad (3)$$

The correction factor, G was estimated by using horizontally polarized excitation light. The vertical component ($I_{\perp}$) and horizontal component ($I_{\parallel}$) of the emission were accumulated through the emission monochromator when the emission polarizer was fixed vertically and horizontally, respectively. For our TCSPC setup, G = 0.6.

2.2.8. Fluorescence Correlation Spectroscopy Study. FCS measurements of cholesterol−SDS and cholesterol−CTAB solution mixtures were carried out using DCS 120 Confocal Laser Scanning Microscope (CLSM) system (Becker & Hickl DCS-120) with inverted optical microscope of Zeiss (Carl Zeiss, Germany).

The correlation function $G(\tau)$, which was used to describe the temporal fluctuation of fluorescence intensity is defined as[34,35]

$$G(\tau) = \frac{\langle \delta F(t)\delta F(t+\tau)\rangle}{\langle F(t)\rangle^2} \quad (4)$$

where $\delta F(t)$ represents the fluctuation of fluorescence signal $F(t)$ as deviations from the temporal average of the signal $\langle F\rangle$ at time t. Therefore, $\delta F(t) = F(t) - \langle F\rangle$.

The detailed descriptions related to experimental section (instrumentation and solution preparation) are given in Supporting Information.

3. RESULTS AND DISCUSSION

3.1. Structural Characterizations of Surfactant and Cholesterol-Containing Nanoaggregates. *3.1.1. Phase Behavior Study.* In aqueous solution, SDS molecules form micelles (average diameter ∼1 nm). However, visual change in phase behavior is observed with the addition of cholesterol (variation of Q value, i.e., concentration of cholesterol, from 0 to 1) in aqueous solution of SDS. We have measured turbidity of the solution mixtures by monitoring the absorbance of individual solution mixtures at 500 nm. In micellar solution (i.e., Q = 0.00), the optical density value is almost '0' as the micellar assemblies are unable to scatter light at this particular wavelength (500 nm). The absorbance of the solution mixture increases gradually from Q = 0.05 to Q = 1.00. This variation in turbidity provides an initial idea about the transition of surfactant micelle to vesicle. With increase in cholesterol concentration, the systems contain vesicular aggregates and exhibit higher absorbance. The variation of turbidity of cholesterol−SDS solution mixtures is almost similar to that of cholesterol−CTAB solution mixtures (Figure 1). The turbidity

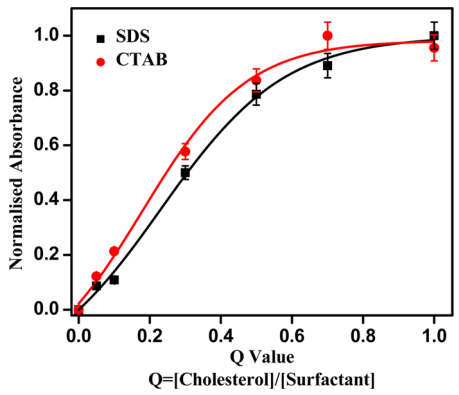

Figure 1. Variation of turbidity of (i) cholesterol−SDS (■) and (ii) cholesterol−CTAB (●) self-assembly with increasing Q values (Q = [cholesterol]/[surfactant]).

of the solution mixtures increases sharply up to Q = 0.50, and after Q=0.70, it becomes saturated. This variation of turbidity in cholesterol−SDS and cholesterol−CTAB solution mixtures with increase in cholesterol content can be easily understood from the photographs of the solution mixtures shown in Figure S1 (Supporting Information).

DOI: 10.1021/la504819v
Langmuir 2015, 31, 2310−2320

3.1.2. Dynamic Light Scattering Measurements. The micelle−vesicle transition of aqueous SDS solution with increase in cholesterol concentration was also characterized by DLS measurement. The intensity−size distribution profiles of SDS micelles (Q = 0.00) and cholesterol−SDS vesicles are shown in Figure 2. The DLS profiles suggest that the diameter

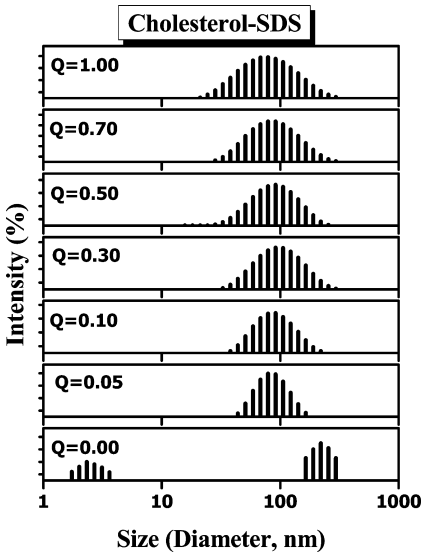

Figure 2. DLS intensity-size distribution histogram of supramolecular assemblies present in cholesterol−SDS mixtures in water at different Q values.

of each SDS micelle is around ∼1 nm, although an intense peak (minor population) in the larger diameter range is also noticed, owing to the presence of larger aggregates. As the light scattering intensity ($I_{scatter}$) is proportional to the sixth power of the diameter of particles (d^6), this intense peak is observed in the larger diameter range (i.e., at minor population). However, the size of the aggregates increases up to ∼80−130 nm in diameter with the addition of cholesterol, suggesting the transformation of surfactant micelles to vesicles. Similar observation was also reported previously from size distribution profiles of cationic surfactant and cholesterol-containing supramolecular assemblies.[27,29,30] It can be concluded that similar to cholesterol and cationic surfactant aggregates, at lower Q value, micelles, mixed micelles, and vesicles are present together in the mixture of cholesterol−SDS supramolecular aggregates. Therefore, with addition of cholesterol, the smaller micelles are not observed in DLS profiles, as scattering intensity ($I_{scatter}$) is proportional to the sixth power of the diameter (d^6) of aggregates. Further, we have characterized the shape and morphology of an equimolar mixture of SDS and cholesterol aggregates by cryo-TEM images.

To observe the stability of cholesterol−SDS-containing vesicles, DLS and UV−vis measurements at Q = 1.00 were also monitored for 7 days. The intensity distribution profiles of cholesterol−SDS aggregates remain almost unaltered during this time span (Figure S2, Supporting Information). Additionally, the UV−vis absorption spectra of these solutions also indicate that the turbidity of the solution mixture remains unchanged. Moreover, the images of vesicle solution clearly suggest that the solution remains homogeneous, i.e., precipitation is not observed (Figure S3, Supporting Information). Similar observation is also observed in cholesterol−CTAB-containing aggregates (Figure S3, Supporting Information). These observations clearly suggest that the cholesterol and surfactant-containing vesicles are stable at room temperature (27 °C).

3.1.3. Cryogenic Transmission Electron Microscopy Measurements. The morphology of cholesterol−CTAB aggregates is reported at different Q values.[27] Cryo-TEM images of cholesterol−CTAB solution indicate the formation of almost uniformly distributed spherical unilamellar vesicles in an equimolar mixture of CTAB and cholesterol. However, at lower Q values, disk-like or worm-like mixed micelles are also present. Therefore, to gain further insight about the size and morphology of cholesterol−SDS aggregates, we performed cryo-TEM measurements at two different Q values. The cryo-TEM images of cholesterol−SDS aggregates at two different Q values are depicted in Figure 3 (Figure 3a,b: Q = 0.70; Figure 3c,d: Q = 1.00). Cryo-TEM images clearly indicate the formation of uniformly distributed unilamellar spherical vesicles at Q = 1.00. However, at lower Q value (Q = 0.70; Figure 3c,d), disk-like mixed micelles are also present along with spherical vesicles. Cholesterol incorporation in micellar assemblies changes the radius of curvature, which facilities the formation of elongated micelles or cylindrical micelles. Further, increase in cholesterol concentration favors the formation of a vesicle bilayer. In cholesterol−SDS assemblies at Q = 0.70, the presence of disk-like mixed micelles along with closed vesicle is observed. The probable reason for the formation of disk-like mixed micelles is edge-to-edge fusion or growth of the bilayer. In an equimolar mixture of cholesterol and surfactant, the formation of closed bilayer structure, i.e., a vesicle, is thermodynamically favored. This scenario can be explained by assuming the joining of disk-like bilayer assemblies to form closed spherical vesicles.

Additionally, to confirm the formation of spherical vesicles in cholesterol−CTAB solution, we also performed TEM measurements at Q=1.00. The TEM images are shown in Figure S4

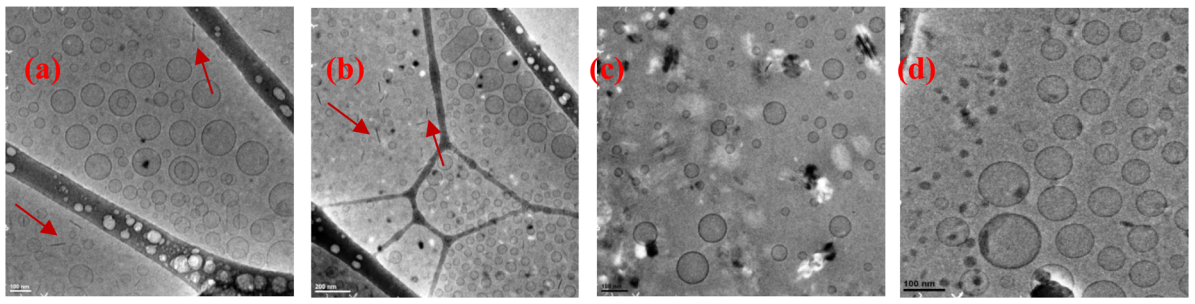

Figure 3. Cryo-TEM images of cholesterol−SDS aggregates at (a,b) Q = 0.70 and (c,d) Q = 1.00).

DOI: 10.1021/la504819v
Langmuir 2015, 31, 2310−2320

(Supporting Information), which clearly indicates the formation of spherical vesicles.

3.1.4. Steady State Anisotropy (r_0) Measurements. Morphology changes of surfactant aggregates, i.e., micelle−vesicle transitions of cholesterol−SDS solution mixtures, are also indicated by the changes in anisotropy (r_0) values of DPH, a membrane bound probe. DPH is a hydrophobic molecule; therefore, the increased hydrophobicity reflects on its rotational motion. The variation of steady-state anisotropy (Figure 4)

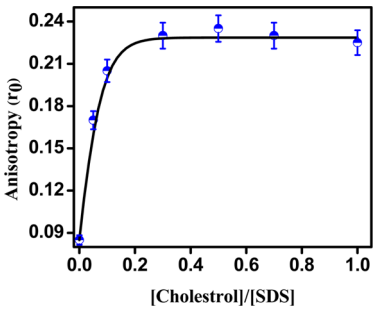

Figure 4. Variation of steady-state anisotropy (r_0) of DPH in supramolecular assemblies of cholesterol−SDS mixtures in water at different Q values.

further suggests the transformation of surfactant micelles to vesicles with the addition of cholesterol. We have also monitored the variation of steady state anisotropy (r_0) in cholesterol−CTAB supramolecular assemblies (Figure S5, Supporting Information) for comparison between cholesterol−CTAB and cholesterol−SDS assemblies. In both of these systems, the anisotropy value increases sharply up to $Q = 0.30$ and then becomes saturated.

The water-insoluble cholesterol molecules remain in the bilayer region of the vesicle; as a result, the hydrophobicity of the vesicle bilayer increases significantly. When the concentration of cholesterol is low, mixed micelles along with very few vesicles are formed by surfactant molecules with the interaction of cholesterol. As the cholesterol content increases further, almost all of the aggregates are transformed into unilamellar vesicles. The observed variation of r_0 values with increase in Q is nicely correlated to the above-mentioned proposal related to cholesterol-induced micelle−vesicle transition in these two systems.

3.1.5. Zeta Potential (ξ) Measurements. The surface charge of the cholesterol-containing vesicles is measured by a zeta potential (ξ) study. Zeta potential is defined as the difference of electrical potential between the stationary layer at the surface of aggregates and the dispersion medium. The dispersion medium extends from the surface of the aggregates owing to the thermal motion of water molecules.

The surface of CTAB micelles is positively charged (43.5 ± 4 mV), whereas the surface charge of SDS micelles is negative (-15.2 ± 3.5 mV). A sharp variation of ξ value is observed with the addition of cholesterol in aqueous micellar solution, i.e., the ξ value becomes more negative in cholesterol−SDS assemblies and more positive in cholesterol−CTAB assemblies at $Q = 0.05$. Upon further increase in cholesterol content, a slight increase (numerical value) in ξ value is observed. Cholesterol molecules are neutral, and the incorporation of cholesterol into micellar aggregates transformed them into larger aggregates (mainly vesicles). The neutral cholesterol molecules also minimize the electrostatic repulsion between the headgroup of surfactant molecules. Therefore, in vesicles, simply more surfactant molecules are densely packed. As a result, the surface charge of vesicles increases significantly (Figure 5). However, at higher cholesterol content, the surface charge decreases (numerical value) slightly.

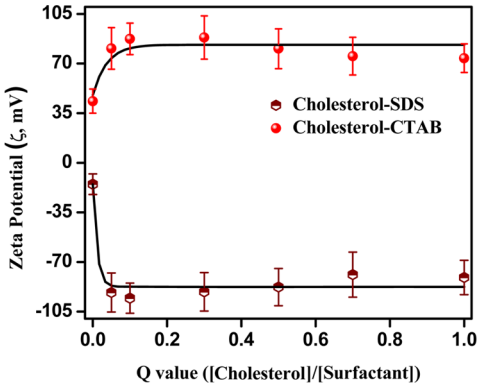

Figure 5. Variation of surface charge (zeta potential, ζ) of supramolecular assemblies of cholesterol−SDS and cholesterol−CTAB mixtures in water with increasing cholesterol concentration (different Q values).

In the next section, we will discuss how the surface charge of vesicles influence the steady state spectral profiles, time-resolved anisotropy and diffusion motion of a hydrophilic dye molecule, rhodamine 6G perchlorate (R6G ClO_4). The shape and size of cholesterol-SDS and cholesterol-CTAB aggregates are almost identical; therefore, it will be interesting to observe the rotational dynamics and diffusion of R6G molecules in these aggregates with increase in cholesterol concentration.

3.2. Effect of Cholesterol on Rotation and Diffusion of R6G Molecules in Cholesterol and Surfactant-Containing Nanoaggregates. *3.2.1. Steady-State Studies.* Initially, the absorption and emission spectra of R6G were monitored in cholesterol−SDS and cholesterol−CTAB assemblies to check how the probe molecules experienced the change in microenvironment as a function of cholesterol content (Q value). The normalized absorption and emission spectra of R6G in these two systems are depicted in Figure 6. The absorption and emission spectral profiles of R6G in aqueous medium are also included in Figure 6 to compare the location of probe molecules in water and that in organized assemblies. According to Figure 6, the red shifts in absorption and emission spectra of R6G in SDS and CTAB (i.e., $Q = 0.00$) micelles clearly suggest that the R6G molecules are solubilized in both micellar assemblies. However, it is interesting to observe the spectral behavior of R6G molecules with the addition of cholesterol in micellar solution. Successive addition of cholesterol induces blue shifts in absorption and emission spectra of R6G in cholesterol−CTAB mixtures, whereas slight red shifts in both spectral profiles are observed in cholesterol−SDS assemblies. In cholesterol−CTAB aggregates, at $Q = 1.00$, the absorption and emission profiles of R6G are the same as that in water. However, in cholesterol−SDS-containing solutions, at the highest cholesterol content (i.e., $Q = 1.00$), the absorption and emission maxima of R6G become ∼535 nm and ∼568 nm, respectively. The variation of excitation spectra of R6G in both aggregates with increasing cholesterol concentration is also identical to that of the absorption spectra (Figure S6, Supporting Information). The dipole moment of R6G

DOI: 10.1021/la504819v
Langmuir 2015, 31, 2310−2320

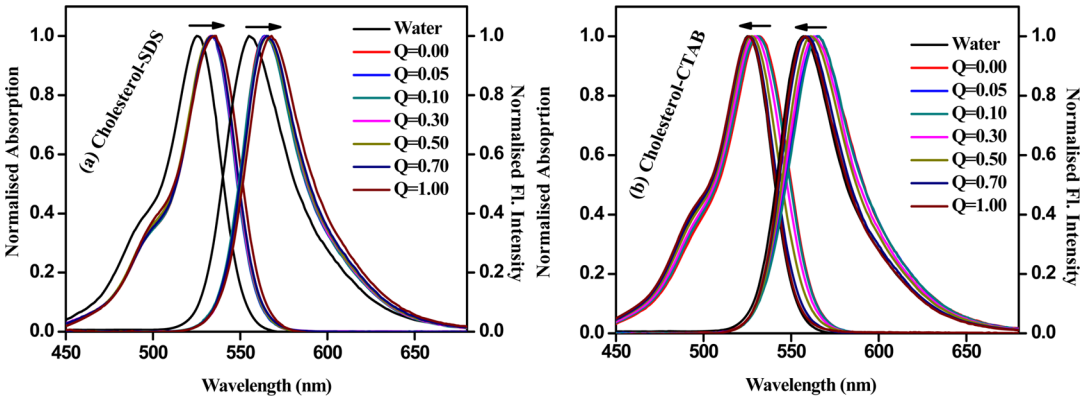

Figure 6. Variation of steady-state absorption and emission spectra of R6G in (a) cholesterol−SDS and (b) cholesterol−CTAB solution at different Q values. The steady-state absorption and emission spectra of R6G in water are also included for comparison.

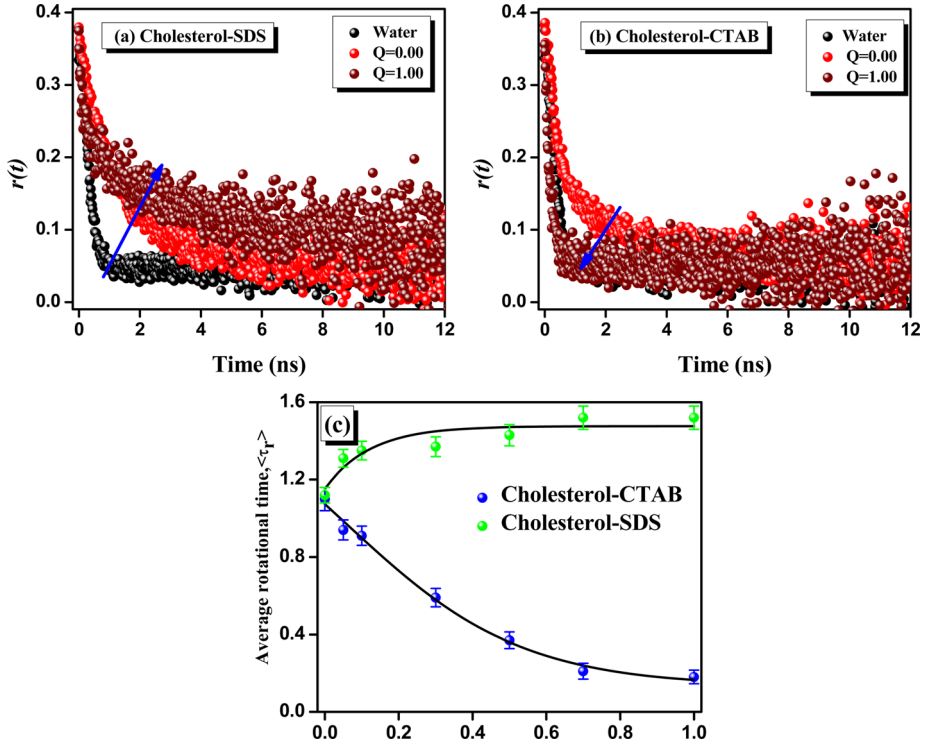

Figure 7. Anisotropy decays of rhodamine 6G in (a) cholesterol−SDS, (b) cholesterol−CTAB solutions at Q = 0.00 and Q = 1.00, and (c) variation of average rotational times ($\langle\tau_r\rangle$) with increasing cholesterol concentration (at different Q values). The anisotropy decay of R6G in water also included in panels a and b for comparison (λ_{ex} = 440 nm).

derivatives is greater in the excited state than in the ground state in isotropic solvent.[36] Therefore, it is expected that the excited state of dye molecules stabilizes more in polar solvent, and red-shifted absorption and emission bands should be observed. However, the opposite trend is observed in reality. The absorption and emission spectra of R6G become red-shifted in micellar solution of SDS and CTAB compared to water. Similar observation in steady-state spectra profiles are also reported for rhodamine derivatives in long-chain alcohols.[37] The hydrogen bonding capability between the amino end group of the dye and protic solvent is increased with increase in the proton donor ability of solvent. The protic solvent acts as a hydrogen bond donor, and the lone pair of the terminal amino group behaves as a hydrogen bond acceptor. As a result, the conjugation between the amino group and the aromatic moiety of the dye is reduced. The hydrogen-bonding interaction involving the lone pair of the terminal nitrogen atom is more significant in water than in other solvents. As a consequence, sometimes the planarity of the molecular skeleton is reduced in both the ground and relaxed excited states, and, accordingly, a blue shift in the absorption and emission spectra of the dye molecule is observed in water compared to that in alcohols. In micellar solution, the accessibility of water around the R6G molecules decreases significantly, and therefore the absorption and emission spectra become red-shifted in micellar solution.

The zeta potential measurement indicates that the surface charge of a cholesterol−CTAB vesicle is more positive and that of a cholesterol−SDS vesicle is more negative than individual micelle solutions. In addition, the presence of cholesterol molecules enhances the hydrophobicity of the vesicle bilayer as indicated in earlier literature by observing the absorption and

DOI: 10.1021/la504819v
Langmuir 2015, 31, 2310−2320

emission spectra of a hydrophobic molecule (C-153) in cationic surfactant and cholesterol aggregates.[30] Since R6G is a cationic molecule, the electrostatic interaction with the surface charge of the vesicle bilayer also plays a significant role in this aspect. R6G molecules are capable of binding at the surface of CTAB micelles, since in CTAB micelles ($Q = 0.00$) the surface charge is not very high. However, in cholesterol−CTAB aggregates, the increased hydrophobicity and surface charge of the vesicle bilayer stimulate the migration of R6G molecules from the bilayer to the aqueous phase, which results in blue-shifted spectral profiles. Additionally, in cholesterol−surfactant aggregates, the hydration of vesicle bilayer decreases significantly with increase in cholesterol concentration.[30] The surface of SDS micelles is negatively charged. The electrostatic attractive interaction preferentially binds R6G molecules at the surface of SDS micelles. As a result, it is found that the absorption and emission spectra of R6G molecules become more red-shifted at Q=1.00 in SDS-containing solution due to the strong binding of R6G at the surface of vesicles. In cholesterol−SDS aggregates, although the hydrophobicity increases with increase in cholesterol content, the increase in surface charge controls the motion of R6G molecules. Therefore, the absorption and emission profiles of R6G molecules in cholesterol-containing vesicle solution can be explained properly considering the hydrophobicity of the vesicle bilayer and the surface charge of the aggregates.

3.2.2. Time-Resolved Anisotropy Measurements. To obtain information regarding the rigidity and hydrophobicity experienced by R6G molecules in surfactant aggregates with increase in cholesterol concentration (i.e., different Q values), we measured the time-resolved fluorescence anisotropy decays. The rotational dynamics of probe molecules in organized assemblies depend on their location and interaction with the surrounding environment.[38−43] The nature (ionic or nonionic) of the organized assemblies is a crucial parameter in determining the location of ionic or hydrophobic dye molecules.[38,39] Therefore, the proper choice of probe molecule and correlation of its rotational motion is helpful in monitoring hydration behavior as well as the solubilization site of dye molecules in organized assemblies. However, in the literature, any comprehensive understanding regarding the rotational motion of hydrophilic dye molecules with the variation of the surface charge of vesicle bilayers has not been reported. Therefore, the anisotropy decays of R6G in cholesterol−CTAB and cholesterol−SDS aggregates were monitored, which provided quantitative information about the migration or entrapment of probe molecules between aggregates and the aqueous phase.

The time-resolved anisotropy decays of R6G in cholesterol−SDS and cholesterol−CTAB (at $Q = 0.00$ and $Q = 1.00$) are depicted in Figure 7a,b, respectively (the anisotropy decays of R6G at all Q values in both aggregates are shown in Figure S7, Supporting Information). Additionally, we have also included the anisotropy decay of R6G in aqueous solution in the same figure for comparison. In aqueous solution, R6G exhibits single exponential decay, but in micellar solutions of CTAB and SDS, the anisotropy decay becomes biexponential. The average rotational time of R6G becomes ∼1.10 ns and ∼1.12 ns in CTAB and SDS micelles, respectively. However, interestingly, with increase in Q value, the anisotropy decays of R6G become slower in cholesterol−SDS aggregates, whereas, in cholesterol−CTAB aggregates, faster anisotropy decays are observed. In cholesterol−CTAB assemblies, at higher Q values ($Q = 0.70$ and $Q = 1.00$), anisotropy decays become single exponential and similar to the anisotropy decay of R6G in water. The parameters of anisotropy decays of R6G in aqueous solution and cholesterol−surfactant mixtures at different Q values are given in Table 1. The variations in the average rotational time constant of R6G in cholesterol−SDS and cholesterol−CTAB assemblies as a function of Q value are shown in Figure 7c. The biexponential anisotropy decay arises because of the various kinds of motion of the probe molecules in the micelle.[43] Generally, the time constant value of the overall rotational motion of the micelle or vesicle is considerably high compared with the value of the slow and fast components of anisotropy decay.[31,39] So, the contribution of the overall rotational motion of vesicles to anisotropy decay is negligible. Thus, the slow and fast components of anisotropy decay mainly correspond to the lateral diffusion or internal motion of probe molecule in micelle. However, in our study, we are mainly focused on the influence of surface charge on the location, i.e., the binding or migration, of R6G in cholesterol−surfactant aggregates with increase in cholesterol concentration. The average rotational time ($\langle\tau_r\rangle$) can provide the exact scenario of the probe location in cholesterol−surfactant aggregates.

Table 1. Dynamic Parameters of Fluorescence Anisotropy of R6G in Aqueous Solution and Cholesterol−Surfactant Mixtures at Different Q Values (λ_{ex} = 440 nm)

system	Q value	$\tau_{fast}(a_{fast})$ (ns)	$\tau_{slow}(a_{slow})$ (ns)	$\langle\tau_r\rangle^a$ (ns)
water		0.26 (1.00)		0.26
cholesterol−CTAB	0.00	0.33 (0.64)	2.46 (0.36)	1.10
	0.05	0.23 (0.65)	2.26 (0.35)	0.94
	0.10	0.22 (0.65)	2.20 (0.35)	0.91
	0.30	0.18 (0.77)	1.96 (0.23)	0.59
	0.50	0.18 (0.87)	1.61 (0.13)	0.37
	0.70	0.27 (1.00)		0.27
	1.00	0.25 (1.00)		0.25
cholesterol−SDS	0.00	1.00 (0.13)	1.14 (0.87)	1.12
	0.05	0.40 (0.35)	1.80 (0.65)	1.31
	0.10	0.38 (0.36)	1.90 (0.64)	1.35
	0.30	0.36 (0.39)	2.01 (0.61)	1.37
	0.50	0.30 (0.37)	2.10 (0.63)	1.43
	0.70	0.16 (0.43)	2.54 (0.57)	1.52
	1.00	0.15 (0.54)	3.12 (0.46)	1.52

[a]Experimental error ∼ 5%.

The observed variation in anisotropy decays can be explained by considering the increased hydrophobicity of the vesicle bilayer with addition of cholesterol and the electrostatic interaction between the charged surface of the vesicle and the probe molecule. As mentioned earlier, the surface of cholesterol−SDS vesicles is negatively charged, whereas that of cholesterol−CTAB vesicles is positively charged. Therefore, electrostatic attraction between the oppositely charged species (vesicle bilayer and probe molecule) is responsible for the binding of the probe molecules in the bilayer; therefore, the rotational relaxation time of R6G increases significantly in cholesterol−SDS vesicles. The increase in cholesterol concentration induces the formation of uniformly distributed spherical vesicles. However, in cholesterol−CTAB vesicles, the electrostatic repulsion of R6G with the surface charge of vesicles along with the increased hydrophobicity of the vesicle bilayer influence the migration of R6G to aqueous phase. As a consequence, the rotational time of R6G decreases significantly

DOI: 10.1021/la504819v
Langmuir 2015, 31, 2310−2320

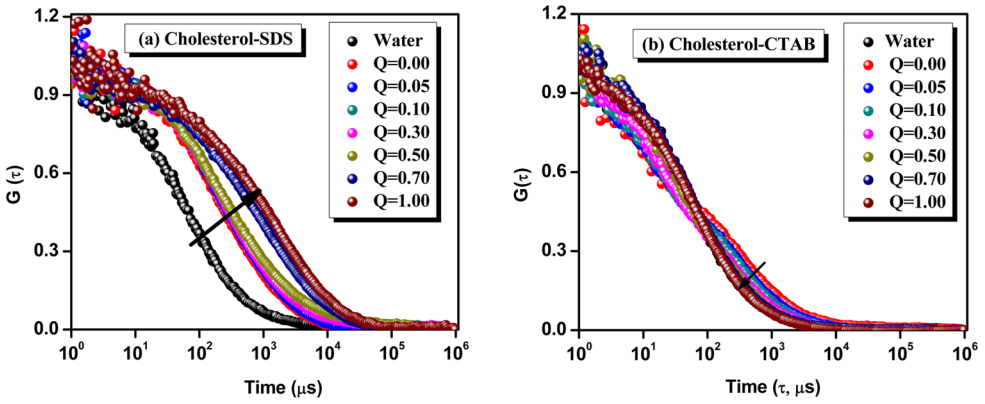

Figure 8. FCS traces of R6G in water, cholesterol−SDS and cholesterol−CTAB, aggregates at different Q values.

and becomes single exponential at higher concentrations of cholesterol. Since R6G is a water-soluble cationic dye molecule, the surface charge of vesicles controls the binding or migration of it between the vesicle surface and the aqueous phase.

3.2.3. Diffusion of R6G in Cholesterol−SDS and Cholesterol−CTAB Assemblies. To gain better insight about the translational diffusion of R6G in vesicles, we have applied the FCS technique, which successfully provides information about the dynamic properties of the organized assemblies. In the FCS technique, the fluctuations of emission intensity of a fluorophore within a small observation volume (~1 fL), i.e., the single-molecular level, are observed. The autocorrelation function is generated using these intensity fluctuations.[34] In recent times, FCS has been an emerging technique to study the diffusion of organic dye molecules, chemical kinetics, or the conformational changes of biomolecules in liquid or organized assemblies.[44−57] Additionally, the aggregation of surfactant molecules in aqueous and nonaqueous solvent is also investigated using this technique.[58−63]

The diffusion coefficient of dye molecules depends upon the morphology, size, and structural heterogeneity of organized assemblies. If we consider a single vesicle, then depending upon the location of probe molecules, multiple values of diffusion coefficient can be obtained.[60] Therefore, in the present study, we are interested in correlating how the surface charge and hydrophobicity of a vesicle bilayer control the translational diffusion motion of an R6G molecule at the single-molecular level. Therefore, in this section, the diffusion property of R6G molecules is investigated during spontaneous transition of micelle to vesicle in aqueous cholesterol−surfactant aggregates with increase in cholesterol content. By comparing the diffusion coefficient (D_t) of the dye molecule in cholesterol−SDS and cholesterol−CTAB aggregates, it is possible to understand the binding interaction between R6G and vesicle aggregates.

The autocorrelation curves of R6G in cholesterol−SDS and cholesterol−CTAB aggregates are shown in Figure 8. For comparison, the FCS curve of R6G in water is also shown in the same figure. We have fitted the FCS trace in water using a one-species fitting equation with a D_t value of ~426 $\mu m^2 s^{-1}$. In cholesterol−SDS aggregates, a multiple-species fitting equation is used to fit the experimentally obtained FCS traces and to obtain the best possible results. As cationic R6G molecules are water-soluble, we fixed the D_t value of R6G in water and evaluated the other component during FCS curve fitting. The obtained diffusion coefficient value is much less than that of water, and it is due to R6G entrapped in SDS micelles or vesicle bilayers. With increase in cholesterol concentration, the D_t value decreases significantly. The size of the aggregates is around ~100 nm, which is much less than the spatial resolution of the microscope (~250 nm for λ_{ex} = 488 nm). Therefore, the smaller diffusion coefficient values can be ascribed to the movement of the micelle or vesicle as a whole. At higher Q values, the solution mixture contains uniformly distributed vesicles; as a result, the D_t value increases significantly. However, in CTAB micelles, a fast diffusion time (τ_D = ~10 μs) of R6G along with a slow component is observed. This slow component (τ_D) corresponds to dye encapsulated in micelles. The fast component may arise due to triplet contribution. We are only interested in observing the variation in diffusion coefficient of R6G encapsulated in cholesterol−surfactant aggregates at different concentrations of cholesterol. With the addition of cholesterol, the observed diffusion coefficient (D_t) value increases in cholesterol−CTAB aggregates and becomes single exponential at Q = 0.70 and Q = 1.00. The FCS traces of R6G in cholesterol−CTAB aggregates at Q = 0.70 and Q = 1.00 are almost similar to FCS traces of the dye in water. The observed diffusion coefficient (D_t) values in cholesterol−CTAB and cholesterol−SDS aggregates are given in Table S1. So, it can be viewed as the diffusion coefficient value of R6G in a CTAB micelle (Q=0.00) due to the motion of the micelle, and, at higher cholesterol content (Q = 0.70 and Q = 1.00), the D_t values indicate the diffusion motion of R6G in aqueous phase. Therefore, it can be concluded that FCS measurements clearly indicate the motion of a vesicle in cholesterol−SDS aggregates (at all Q values), but in cholesterol−CTAB solution, at higher Q values (Q = 0.70 and Q = 1.00), the D_t value indicate only the diffusion of R6G in aqueous phase. The fitted FCS curves are shown in Figure S8 (Supporting Information).

Now, from the diffusive nature of R6G in cholesterol−CTAB and cholesterol−SDS aggregates, it is clearly observed that the diffusion coefficient strongly depends on the charge on the surface of vesicles and dye molecules. The diffusional motion of R6G is ~8 times slower in anionic SDS micelles and ~6 times slower in cationic CTAB micelles than in water. As R6G is a cationic dye, the diffusional motion is slowed down more in anionic SDS micelles than in cationic CTAB micelles. However, with the addition of cholesterol, the micelle-to-vesicle transition occurs in aqueous surfactant solution, which influences the diffusion coefficient values of R6G. The diffusion of R6G becomes slow with the addition of cholesterol in SDS solution and, compared with the D_t value of R6G in water, an almost ~33-fold decrease is observed at Q = 1.00. However, the diffusion of R6G becomes faster with addition of cholesterol in

DOI: 10.1021/la504819v
Langmuir 2015, 31, 2310−2320

CTAB solution, and at Q = 1.00, it becomes so fast that it exactly matches with its diffusional motion in pure water. The rigidity of the bilayer increases significantly with addition of cholesterol, and the surface charge (numerical value) of vesicle is also increased. Therefore, due to strong hydrophobicity and the repulsive interaction of the vesicle bilayer with the cationic R6G molecules, they migrate from the bilayer to the aqueous solution. As a result, the D_t value of R6G at Q = 1.00 is almost similar to that of water. In cholesterol−SDS aggregates, the negative surface charge predominates over the increased hydrophobicity of the vesicle bilayer. Therefore, cationic R6G efficiently binds to the bilayer, and observed diffusion times become slower.

4. CONCLUSION

The important outcomes of this article may be summarized as follows: First, we have shown that anionic surfactant, SDS, can form unilamellar stable vesicles in aqueous solution on addition of cholesterol. The formation of unilamellar vesicles with a distinct bilayer in a cholesterol−SDS mixture has been confirmed by cryo-TEM images. Second, a detailed and comparative study regarding the rotational and diffusion motion of a cationic dye molecule, R6G, has been presented. To investigate the influence of the surface charge and hydrophobicity of a bilayer on the binding or migration of R6G molecules, absorption-emission spectra, time-resolved anisotropy, and FCS measurements were monitored in cholesterol−SDS and cholesterol−CTAB aggregates at different Q values. The hydrophobicity of vesicle bilayer and surface charge of bilayer increases significantly in vesicles than micelles. The strong electrostatic interaction between the surface charge of vesicles and probe molecules controls the binding of R6G molecules on the vesicle surface. It is observed that the rotational and diffusion time constants of R6G molecules increase significantly in SDS solution with addition of cholesterol due to the strong electrostatic attractive interaction between the concerned vesicle surface and the probe molecule. However, the rotational and diffusion time constants of R6G decrease significantly with the addition of cholesterol in aqueous solution of CTAB. In higher cholesterol-containing CTAB solution, the rotational and diffusion time constants of R6G molecules are almost similar to those in water. Therefore, in cholesterol−CTAB solution, the electrostatic repulsion between the surface charges on vesicles and R6G molecules as well as the enhanced hydrophobicity of vesicle bilayer induce the migration of hydrophilic R6G molecules from the vesicle bilayer to the aqueous phase. Although both the hydrophobicity and surface charge (numerical value) of the vesicle increase with addition of cholesterol, the surface charge on vesicles controls the motion of R6G molecules.

■ ASSOCIATED CONTENT

Supporting Information

Information on solution preparation, detailed instrumentation, table for diffusion coefficient values, images of cholesterol-surfactant mixtures, DLS profiles, UV-Vis absorption and images of cholesterol-surfactant solution regarding their stability, TEM images of cholesterol-CTAB solution at Q = 1.00, variation in steady state anisotropy of DPH in cholesterol-CTAB solution, excitation spectra of R6G, anisotropy decays of R6G and fitted FCS traces in cholesterol-surfactant solution at all Q values, and are given in the Supporting Information. This material is available free of charge via the Internet at http://pubs.acs.org.

■ AUTHOR INFORMATION

Corresponding Author

*E-mail: nilmoni@chem.iitkgp.ernet.in; Fax: 91-3222-255303; Phone: 91-3222-283332.

Notes

The authors declare no competing financial interest.

■ ACKNOWLEDGMENTS

This article is dedicated to Professor Kankan Bhattacharyya in his 60th year. N.S. is indebted to Professor Kankan Bhattacharyya of IACS, Kolkata for his inspiring words and encouragement to venture into FLIM and FCS. N.S. is also thankful to the SERB, Department of Science and Technology and Council of Scientific and Industrial Research (CSIR), Government of India, for providing generous research grants. S.G. and A.R. are thankful to CSIR for research fellowships. D.B. and N.K. are thankful to IIT Kharagpur for research fellowships. J.K. acknowledges UGC for a research fellowship. We are also thankful to Prof. Anindya Datta and Prof. J. Bellare of IIT Bombay for their help in obtaining cryo-TEM images.

■ REFERENCES

(1) Guo, X.; Szoka, F. C., Jr. Chemical Approaches to Triggerable Lipid Vesicles for Drug and Gene Delivery. *Acc. Chem. Res.* **2003**, *36*, 335−341.

(2) Cevc, G. Lipid Vesicles and Other Colloids as Drug Carriers on the Skin. *Adv. Drug Delivery Rev.* **2004**, *56*, 675−711.

(3) Peetla, C.; Stine, A.; Labhasetwar, V. Biophysical Interactions with Model Lipid Membranes: Applications in Drug Discovery and Drug Delivery. *Mol. Pharmaceutics* **2009**, *6*, 1264−1276.

(4) Pramod, P. S.; Takamura, K.; Chaphekar, S.; Balasubramanian, N.; Jayakannan, M. Dextran Vesicular Carriers for Dual Encapsulation of Hydrophilic and Hydrophobic Molecules and Delivery into Cells. *Biomacromolecules* **2012**, *13*, 3627−3640.

(5) Szoka, F., Jr.; Papahadjopoulos, D. Comparative Properties and Methods of Preparation of Lipid Vesicles (Liposomes). *Annu. Rev. Biophys. Bioeng.* **1980**, *9*, 467−508.

(6) Minami, H.; Inoue, T.; Shimozawa, R. Kinetics of Divalent Cation-Induced and pH-Induced Aggregation of Dimyristoylphosphatidylserine Vesicles. *J. Colloid Interface Sci.* **1994**, *164*, 9−15.

(7) Kaler, E. W.; Murthy, A. K.; Rodriguez, B. E.; Zasadzinski, J. A. Spontaneous Vesicle Formation in Aqueous Mixtures of Single-Tailed Surfactants. *Science* **1989**, *245*, 1371−1374.

(8) Hao, J.; Liu, W.; Xu, G.; Zheng, L. Vesicles from Salt-Free Cationic and Anionic Surfactant Solutions. *Langmuir* **2003**, *19*, 10635−10640.

(9) Yatcilla, M. T.; Herrington, K. L.; Brasher, L. L.; Kaler, E. W.; Chiruvolu, S.; Zasadzinski, J. A. Phase Behavior of Aqueous Mixtures of Cetyltrimethylammonium Bromide (CTAB) and Sodium Octyl Sulfate (SOS). *J. Phys. Chem.* **1996**, *100*, 5874−5879.

(10) Kato, K.; Walde, P.; Koine, N.; Ichikawa, S.; Ishikawa, T.; Nagahama, R.; Ishihara, T.; Tsujii, T.; Shudou, M.; Omokawa, Y.; Kuroiwa, T. Temperature-Sensitive Nonionic Vesicles Prepared from Span 80 (Sorbitan Monooleate). *Langmuir* **2008**, *24*, 10762−10770.

(11) Tian, M.; Zhu, L.; Yu, D.; Wang, Y.; Sun, S.; Wang, Y. Aggregate Transitions in Mixtures of Anionic Sulfonate Gemini Surfactant with Cationic Ammonium Single-Chain Surfactant. *J. Phys. Chem. B* **2013**, *117*, 433−440.

(12) Ghosh, S.; Ghatak, C.; Banerjee, C.; Mandal, S.; Kuchlyan, J.; Sarkar, N. Spontaneous Transition of Micelle-Vesicle-Micelle in a mixture of Cationic Surfactant and Anionic Surfactant like Ionic Liquid: A Pure Non-lipid Small Unilamellar Vesicular Template Used

DOI: 10.1021/la504819v
Langmuir 2015, 31, 2310−2320

for Solvent and Rotational Relaxation Study. *Langmuir* **2013**, *29*, 10066−10076.
(13) Cano-Sarabia, M.; Angelova, A.; Ventosa, N.; Lesieur, S.; Veciana, J. Cholesterol Induced CTAB Micelle-to-Vesicle Phase Transitions. *J. Colloid Interface Sci.* **2010**, *350*, 10−15.
(14) Davies, T. S.; Ketner, A. M.; Raghavan, S. R. Self-Assembly of Surfactant Vesicles that Transform into Viscoelastic Wormlike Micelles upon Heating. *J. Am. Chem. Soc.* **2006**, *128*, 6669−6675.
(15) Li, W.; Yang, Y.; Luo, T.; Zhang, Z.; Han, B. CO_2-Induced Micelle to Vesicle Transition in Zwitterionic−Anionic Surfactant Systems. *Phys. Chem. Chem. Phys.* **2014**, *16*, 3640−3647.
(16) Wu, Z.; Yan, Y.; Huang, J. Advanced Molecular Self-Assemblies Facilitated by Simple Molecules. *Langmuir* **2014**, *30*, 14375−14384.
(17) Wang, H.; Tan, B.; Wang, J.; Li, Z.; Zhang, S. Anion-Based pH Responsive Ionic Liquids: Design, Synthesis, and Reversible Self-Assembling Structural Changes in Aqueous Solution. *Langmuir* **2014**, *30*, 3971−3978.
(18) Sagar, G. H.; Bellare, J. R. Estimation of Mechanical Strength of Unilamellar and Multilamellar AOT/Water Vesicles and Their Rupture Using Micropipet Aspiration. *J. Phys. Chem. B* **2009**, *113*, 13805−13810.
(19) De, D.; Sajjan, M.; Narayanan, J.; Bellare, J. R.; Datta, A. Nanoconfinement of Water Layers in Lamellar Structures Prepared in the Presence and Absence of Organic Solvent. *J. Phys. Chem. B* **2013**, *117*, 2106−2112.
(20) Rao, K. S.; Singh, T.; Kumar, A. Aqueous-Mixed Ionic Liquid System: Phase Transitions and Synthesis of Gold Nanocrystals. *Langmuir* **2011**, *27*, 9261−9269.
(21) Kumar, G. P.; Rajeshwarrao, P. Nonionic Surfactant Vesicular Systems for Effective Drug Delivery—An Overview. *Acta Pharmaceutica Sinica B* **2011**, *1*, 208−219.
(22) Fendler, J. H.; Hinze, W. L. Reactivity Control in Micelles and Surfactant Vesicles. Kinetics and Mechanism of Base-Catalyzed Hydrolysis of 5,5′-Dithiobis(2-nitrobenzoic acid) in Water, Hexadecyltrimethylammonium Bromide Micelles, and Dioctadecyldimethylammonium Chloride Surfactant Vesicles. *J. Am. Chem. Soc.* **1981**, *103*, 5439−5441.
(23) Sonnino, S.; Prinetti, A.; Mauri, L.; Chigorno, V.; Tettamanti, G. Dynamic and Structural Properties of Sphingolipids as Driving Forces for the Formation of Membrane Domains. *Chem. Rev.* **2006**, *106*, 2111−2125.
(24) Dolder, M.; Engel, A.; Zulauf, M. The Micelle to Vesicle Transition of Lipids and Detergents in the Presence of a Membrane Protein: Towards a Rationale for 2D Crystallization. *FEBS Lett.* **1996**, *382*, 203−208.
(25) Jiang, L.; Wang, K.; Deng, M.; Wang, Y.; Huang, J. Bile Salt-Induced Vesicle-to-Micelle Transition in Catanionic Surfactant Systems: Steric and Electrostatic Interactions. *Langmuir* **2008**, *24*, 4600−4606.
(26) Yin, H.; Lei, S.; Zhu, S.; Huang, J.; Ye, J. Micelle-to-Vesicle Transition Induced by Organic Additives in Catanionic Surfactant Systems. *Chem.—Eur. J.* **2006**, *12*, 2825−2835.
(27) Ferrer-Tasies, L.; Moreno-Calvo, E.; Cano-Sarabia, M.; Aguilella-Arzo, M.; Angelova, A.; Lesieur, S.; Ricart, S.; Faraudo, J.; Ventosa, N.; Veciana, J. Quatsomes: Vesicles Formed by Self-Assembly of Sterols and Quaternary Ammonium Surfactants. *Langmuir* **2013**, *29*, 6519−6528.
(28) Manosroi, A.; Wongtrakul, P.; Manosroi, J.; Sakai, H.; Sugawara, F.; Yuasa, M.; Abe, M. Characterization of Vesicles Prepared with Various Non-ionic Surfactants Mixed with Cholesterol. *Colloids Surf., B* **2003**, *30*, 129−138.
(29) Mandal, S.; Banerjee, C.; Ghosh, S.; Kuchlyan, J.; Sarkar, N. Modulation of the Photophysical Properties of Curcumin in Nonionic Surfactant (Tween-20) Forming Micelles and Niosomes: A Comparative Study of Different Microenvironments. *J. Phys. Chem. B* **2013**, *117*, 6957−6968.
(30) Mandal, S.; Kuchlyan, J.; Ghosh, S.; Banerjee, C.; Kundu, N.; Banik, D.; Sarkar, N. Vesicles Formed in Aqueous Mixtures of Cholesterol and Imidazolium Surface Active Ionic Liquid: A Comparison with Common Cationic Surfactant by Water Dynamics. *J. Phys. Chem. B* **2014**, *118*, 5913−5923.
(31) Ghosh, S.; Kuchlyan, J.; Roychowdhury, S.; Banik, D.; Kundu, N.; Roy, A.; Sarkar, N. Unique Influence of Cholesterol on Modifying the Aggregation Behavior of Surfactant Assemblies: Investigation of Photophysical and Dynamical Properties of 2,2′-Bipyridine-3,3′-diol, $BP(OH)_2$ in Surfactant Micelles, and Surfactant/Cholesterol Forming Vesicles. *J. Phys. Chem. B* **2014**, *118*, 9329−9340.
(32) Ghosh, S.; Mandal, A. K.; Das, A. K.; Mondal, T.; Bhattacharyya, K. Diffusion of Organic Dyes in a Niosome Immobilized on a Glass Surface Using Fluorescence Correlation Spectroscopy. *Phys. Chem. Chem. Phys.* **2012**, *14*, 9749−9757.
(33) Mondal, T.; Ghosh, S.; Das, A. K.; Mandal, A. K.; Bhattacharyya, K. Salt Effect on the Ultrafast Proton Transfer in Niosome. *J. Phys. Chem. B* **2012**, *116*, 8105−8112.
(34) Lackowicz, J. R. *Principles of Fluorescence Spectroscopy*, 3rd ed.; Springer: New York, 2006.
(35) Hess, S. T.; Webb, W. W. Focal Volume Optics and Experimental Artifacts in Confocal Fluorescence Correlation Spectroscopy. *Biophys. J.* **2002**, *83*, 2300−2317.
(36) Zakerhamidi, M. S.; Moghadam, M.; Ghanadzadeh, A.; Hosseini, S. Anisotropic and isotropic solvent effects on the dipole moment and photophysical properties of rhodamine dyes. *J. Lumin.* **2012**, *132*, 931−937.
(37) Pal, P.; Zeng, H.; Durocher, G.; Girard, D.; Giasson, R.; Blanchard, L.; Gaboury, L.; Villeneuve, L. Spectroscopic and Photophysical Properties of Some New Rhodamine Derivatives in Cationic, Anionic and Neutral Micelles. *J. Photochem. Photobiol., A* **1996**, *98*, 65−72.
(38) Dutt, G. B. Fluorescence Anisotropy of Ionic Probes in AOT Reverse Micelles: Influence of Water Droplet Size and Electrostatic Interactions on Probe Dynamics. *J. Phys. Chem. B* **2008**, *112*, 7220−7226.
(39) Mali, K. S.; Dutt, G. B.; Mukherjee, T. Rotational Diffusion of Organic Solutes in Surfactant-Block Copolymer Micelles: Role of Electrostatic Interactions and Micellar Hydration. *J. Phys. Chem. B* **2007**, *111*, 5878−5884.
(40) Wittouck, N. W.; Negri, R. M.; Ameloot, M.; De Schryver, F. C. AOT Reversed Micelles Investigated by Fluorescence Anisotropy of Cresyl Violet. *J. Am. Chem. Soc.* **1994**, *116*, 10601−10611.
(41) Spry, D. B.; Goun, A.; Glusac, K.; Moilanen, D. E.; Fayer, M. D. Proton Transport and the Water Environment in Nafion Fuel Cell Membranes and AOT Reverse Micelles. *J. Am. Chem. Soc.* **2007**, *129*, 8122−8130.
(42) Krishna, M. M. G.; Srivastava, A.; Periasamy, N. Rotational Dynamics of Surface Probes in Lipid Vesicles. *Biophys. Chem.* **2001**, *90*, 123−133.
(43) Maiti, N. C.; Krishna, M. M. G.; Britto, P. J.; Periasamy, N. Fluorescence Dynamics of Dye Probes in Micelles. *J. Phys. Chem. B* **1997**, *101*, 11051−11060.
(44) Al-Soufi, W.; Reija, B.; Novo, M.; Felekyan, S.; Kuhnemuth, R.; Seidel, C. A. M. Fluorescence Correlation Spectroscopy, a Tool to Investigate Supramolecular Dynamics: Inclusion Complexes of Pyronines with Cyclodextrin. *J. Am. Chem. Soc.* **2005**, *127*, 8775−8784.
(45) Haupts, U.; Maiti, S.; Schwille, P.; Webb, W. W. Dynamics of Fluorescence Fluctuations in Green Fluorescent Protein Observed by Fluorescence Correlation Spectroscopy. *Proc. Natl. Acad. Sci. U.S.A.* **1998**, *95*, 13573−13578.
(46) Sasmal, D. K.; Mondal, T.; Mojumdar, S. S.; Choudhury, A.; Banerjee, R.; Bhattacharyya, K. An FCS Study of Unfolding and Refolding of CPM-Labeled Human Serum Albumin: Role of Ionic Liquid. *J. Phys. Chem. B* **2011**, *115*, 13075−13083.
(47) Yadav, R.; Sengupta, B.; Sen, P. Conformational Fluctuation Dynamics of Domain I of Human Serum Albumin in the Course of Chemically and Thermally Induced Unfolding Using Fluorescence Correlation Spectroscopy. *J. Phys. Chem. B* **2014**, *118*, 5428−5438.
(48) Ishii, K.; Tahara, T. Resolving Inhomogeneity Using Lifetime-Weighted Fluorescence Correlation Spectroscopy. *J. Phys. Chem. B* **2010**, *114*, 12383−12391.

DOI: 10.1021/la504819v
Langmuir 2015, 31, 2310−2320

(49) Yang, J.; Wu, D.; Xie, D.; Feng, F.; Schanze, K. S. Ion-Induced Aggregation of Conjugated Polyelectrolytes Studied by Fluorescence Correlation Spectroscopy. *J. Phys. Chem. B* **2013**, *117*, 16314−16324.
(50) Ishii, K.; Tahara, T. Two-Dimensional Fluorescence Lifetime Correlation Spectroscopy. 2. Application. *J. Phys. Chem. B* **2013**, *117*, 11423−11432.
(51) Pabbathi, A.; Ghosh, S.; Samanta, A. FCS Study of the Structural Stability of Lysozyme in the Presence of Morpholinium Salts. *J. Phys. Chem. B* **2013**, *117*, 16587−16593.
(52) Okumus, B.; Wilson, T. J.; Lilley, D. M. J.; Ha, T. Vesicle Encapsulation Studies Reveal that Single Molecule Ribozyme Heterogeneities Are Intrinsic. *Biophys. J.* **2004**, *87*, 2798−2806.
(53) Benda, A.; Benes, M.; Marecek, V.; Lhotsky, A.; Hermens, W. Th.; Hof, M. How To Determine Diffusion Coefficients in Planar Phospholipid Systems by Confocal Fluorescence Correlation Spectroscopy. *Langmuir* **2003**, *19*, 4120−4126.
(54) Kirkeminde, A. W.; Torres, T.; Ito, T.; Higgins, D. A. Multiple Diffusion Pathways in Pluronic F127 Mesophases Revealed by Single Molecule Tracking and Fluorescence Correlation Spectroscopy. *J. Phys. Chem. B* **2011**, *115*, 12736−12743.
(55) Basak, S.; Chattopadhyay, K. Fluorescence Correlation Spectroscopy Study on the Effects of the Shape and Size of a Protein on Its Diffusion Inside a Crowded Environment. *Langmuir* **2013**, *29*, 14709−14717.
(56) Verma, S. D.; Pal, N.; Singh, M. K.; Shweta, H.; Khan, M. F.; Sen, S. Understanding Ligand Interaction with Different Structures of G-Quadruplex DNA: Evidence of Kinetically Controlled Ligand Binding and Binding-Mode Assisted Quadruplex Structure Alteration. *Anal. Chem.* **2012**, *84*, 7218−7226.
(57) Sahoo, B.; Balaji, J.; Nag, S.; Kaushalya, S. K.; Maiti, S. Protein aggregation probed by two-photon fluorescence correlation spectroscopy of native tryptophan. *J. Chem. Phys.* **2008**, *129*, 075103(1)−075103(5).
(58) Dey, S.; Mandal, U.; Mojumdar, S. S.; Mandal, A. K.; Bhattacharyya, K. Diffusion of Organic Dyes in Immobilized and Free Catanionic Vesicles. *J. Phys. Chem. B* **2010**, *114*, 15506−15511.
(59) Pal, N.; Verma, S. D.; Singh, M. K.; Sen, S. Fluorescence Correlation Spectroscopy: An Efficient Tool for Measuring Size, Size-Distribution and Polydispersity of Microemulsion Droplets in Solution. *Anal. Chem.* **2011**, *83*, 7736−7744.
(60) Orte, A.; Ruedas-Rama, M. J.; Paredes, J. M.; Crovetto, L.; Alvarez-Pez, J. M. Dynamics of Water-in-Oil Nanoemulsions Revealed by Fluorescence Lifetime Correlation Spectroscopy. *Langmuir* **2011**, *27*, 12792−12799.
(61) Zettl, H.; Portnoy, Y.; Gottlieb, M.; Krausch, G. Investigation of Micelle Formation by Fluorescence Correlation Spectroscopy. *J. Phys. Chem. B* **2005**, *109*, 13397−13401.
(62) Narenberg, R.; Kliger, J.; Horn, D. Study of the Interactions between Poly(vinyl pyrrolidone) and Sodium Dodecyl Sulfate by Fluorescence Correlation Spectroscopy. *Angew. Chem., Int. Ed.* **1999**, *38*, 1626−1629.
(63) Ghosh, S.; Adhikari, A.; Mojumdar, S. S.; Bhattacharyya, K. A Fluorescence Correlation Spectroscopy Study of the Diffusion of an Organic Dye in the Gel Phase and Fluid Phase of a Single Lipid Vesicle. *J. Phys. Chem. B* **2010**, *114*, 5736.

DOI: 10.1021/la504819v
Langmuir 2015, 31, 2310−2320